Journal of Chemical&Engineering Data

pubs.acs.org/jced Article

Speed of Sound Measurements of Binary Mixtures of 1,1,1,2-Tetrafluoroethane (R-134a), 2,3,3,3-Tetrafluoropropene (R-1234yf), and *trans*-1,3,3,3-Tetrafluoropropene (R-1234ze(E)) Refrigerants

Aaron J. Rowane* and Richard A. Perkins

Cite This: *J. Chem. Eng. Data* 2022, 67, 1365−1377 Read Online

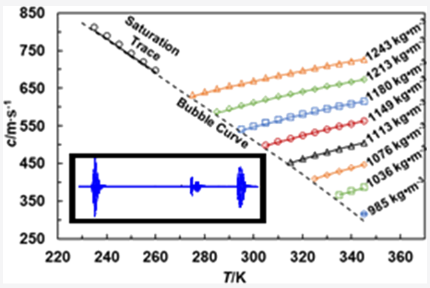

ABSTRACT: Speed of sound data measured using a dual-path pulse-echo instrument are reported for binary mixtures of 1,1,1,2-tetrafluoroethane (R-134a), 2,3,3,3-tetrafluoropropene (R-1234yf), and *trans*-1,3,3,3-tetrafluoropropene (R-1234ze(E)). For each binary mixture, the speed of sound is studied at two compositions of approximately (0.33/0.67) and (0.67/0.33) mole fraction. The conditions covered in this study range in temperature from 230 to 345 K and from pressures slightly above the bubble curve up to a maximum pressure of 51 MPa. However, to avoid potential polymerization reactions, data for mixtures containing R-1234yf are limited to a maximum pressure of 12 MPa at temperatures below 295 K and 8 MPa at temperatures above 295 K. The mean uncertainty of the measured speed of sound is less than 0.1%, where relative combined expanded uncertainties at individual state points range from 0.04 to 0.4% of the measured speed of sound value. The greatest combined expanded uncertainties are encountered as the state point approaches the mixture critical region where weakened echo signals and lower speed of sound values are observed. The reported data are compared to available REFPROP mixture models, which are not adjusted using the data reported here, with average absolute deviations ranging from 0.27 to 0.75% with maximum deviations as high as 1.1%. The comparisons to the REFPROP correlations show that further adjustments to the mixture models are needed to provide a representation of the data within its experimental uncertainty.

1. INTRODUCTION

The discovery of new refrigerants has been driven by toxicity, flammability, reactivity with the ozone layer, and global warming potential (GWP) constraints. Calm[1] and more recently McLinden and Huber[2] outline the history and evolution of refrigerants. Presently, fourth-generation refrigerants, primarily hydrofluoroolefins (HFOs), are being proposed as low GWP alternatives to widely used third-generation refrigerants which are typically hydrofluorocarbons (HFCs). A couple of examples of widely used HFC refrigerants are R-410a, a 50/50 wt % blend of difluoromethane (R-32) and pentafluoroethane (R-125), and 1,1,1,2-tetrafluoroethane (R-134a). Myhre and Shindell[3] provide an extensive list of 100 year GWP values for refrigerants which are 677, 3170, and 1300 for R-32, R-125, and R-134a, respectively. Proposed fourth-generation refrigerants, HFOs such as 2,3,3,3-tetrafluoropropene (R-1234yf) and *trans*-1,3,3,3-tetrafluoropropene (R-1234ze(E)), have 100 year GWP values of less than 1. However, "fourth-generation" refrigerants such as R-1234yf and R-1234ze(E) exhibit shortcomings in their performance, are moderately flammable compared to third-generation refrigerants,[4,5] and as highlighted by Luecken et al. HFOs such as R-1234yf break down into trifluoroacetic acid at a much faster rate than HFCs such as R-134a. Therefore, third- and fourth-generation blends are an alternative used to obtain a product with a lower GWP than "third-generation" refrigerants that is less flammable[6] than "fourth-generation" refrigerants while still providing the necessary level of efficiency for their application.

The design and optimization of refrigeration and air conditioning components are reliant on accurate equations of state (EoS) for refrigerants and their mixtures. Studies such as that by Bobbo et al.[7] review the available thermodynamic and transport property data for pure refrigerants and briefly catalog the properties of refrigerant mixtures. A more recent survey of refrigerant fluid property data and models for mixtures by Bell and colleagues[8] shows that several studies report density,[9−13] heat capacity,[9] vapor−liquid equilibrium,[14,15] and critical property data[10,16] for mixtures of HFC and HFO refrigerants. However, of the available literature, only a single study by Shimoura et al.[17] reports liquid-phase speed of sound data for refrigerant mixtures. Further, Shimoura et al. report a single composition for each mixture, limiting the validation possible

Received: January 18, 2022
Accepted: April 18, 2022
Published: May 17, 2022

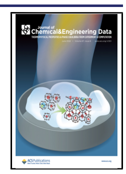

Table 1. Refrigerant Samples Used in This Study Listed with Their CAS Numbers, Molar Mass, Source, Purity, and GWP_{100} Values Reported by Myhre and Shindell[3a]

chemical name	CAS number	molar mass/g·mol^{-1}	source	purity/mole fraction	GWP_{100}
1,1,1,2-tetrafluoroethane (R-134a)	811-97-2	102.03	Dupont	0.999	1300
2,3,3,3-tetrafluoropropene (R-1234yf)	754-12-1	114.04	Chemours; Opteron	0.9999	<1
trans-1,3,3,3-tetrafluoropropene (R-1234ze(E))	29118-24-9	114.04	Honeywell	0.9997	<1

[a]All samples were degassed using a freeze−pump−thaw method prior to preparing mixtures.

Table 2. Binary Mixture Compositions for R-1234yf, R-134a, and R-1234ze(E) Listed with Total Sample Mass Prepared and the Combined Expanded Uncertainties of the Mole Fractions with a Coverage Factor, k = 2

mixture	composition/mole fraction	sample mass/g	$U_c(x_1)$/mole fraction
R-1234yf/134a	0.33634/0.66366	312.6626	0.00010
R-1234yf/134a	0.66759/0.33241	332.2073	0.00010
R-1234yf/1234ze(E)	0.33584/0.66416	335.2690	0.00010
R-1234yf/1234ze(E)	0.66660/0.33340	342.9511	0.00010
R-134a/1234ze(E)	0.32916/0.67084	110.8245	0.00010
R-134a/1234ze(E)	0.67102/0.32898	88.3572	0.00010

for mixture EoS models. The motivation of the present work is to expand the experimental knowledge of mixtures with third- and fourth-generation refrigerants. Therefore, this study reports new speed of sound data measured for mixtures of one third-generation refrigerant, R-134a, with two prominent fourth-generation refrigerants, R-1234yf and R-1234ze(E), at temperatures from 230 to 345 K and pressures up to 12 MPa for mixtures containing R-1234yf and pressures up to 51 MPa for R-134a/1234ze(E) mixtures. Measurements with R-1234yf were limited to 12 MPa to avoid potential polymerization reactions previously observed by Richter et al.[18]

The measurement of caloric thermodynamic properties such as the heat capacity, which are needed to determine the overall heat transfer coefficient of heat exchangers, can be challenging at high pressures with a low experimental uncertainty. However, as described by Lin and Trusler,[19] speed of sound data can be fit to an EoS and used to determine a variety of thermodynamic properties such as the heat capacity, density, and thermal expansivity within reasonable uncertainties. Currently, REFPROP (version 10.0)[20] is equipped with mixture Helmholtz-energy-explicit EoS for R-134a,[21] R-1234yf,[22] and R-1234ze(E),[23] which use binary interaction parameters and mixing rules described by Bell and Lemmon.[24] Bell et al.[8] report binary interaction parameters for a variety of refrigerants including those originally quoted by Lemmon for R-1234yf/134a, R-1234yf/1234ze(E), and R-134a/1234ze(E) mixtures. However, due to the absence of experimental speed of sound data for R-134a, R-1234yf, and R-1234ze(E) binary mixtures, the performance of the REFPROP refrigerant mixture models to predict the speed of sound of these mixtures has remained untested. Therefore, the data reported in the present study is used to test the performance of the current mixture Helmholtz-energy-explicit EoS for these refrigerants.

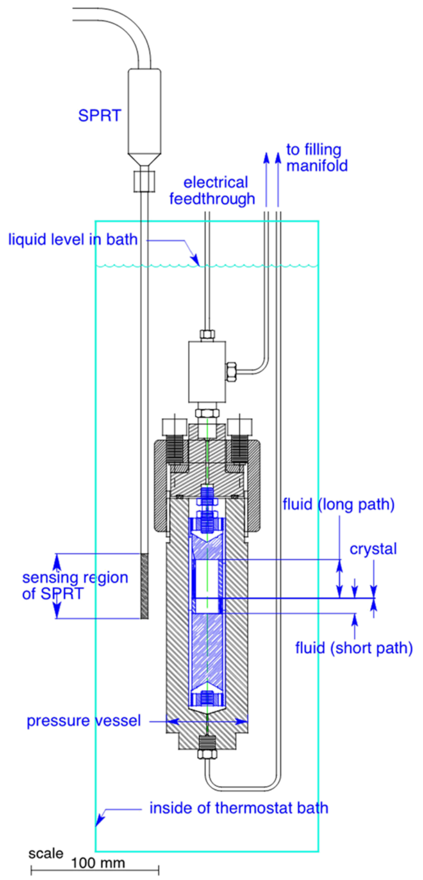

Figure 1. Schematic diagram for the main components of the pulse-echo apparatus.

2. EXPERIMENTAL SECTION

2.1. Materials and Methods. Table 1 lists the refrigerants used in this study along with their short names, CAS numbers, molar mass, source, and purity. Prior to preparing mixtures, each pure component was degassed using a freeze−pump−thaw method. First, liquid samples, as received from the manufacturer, were transferred to stainless steel sample cylinders. The sample cylinders were then connected to a high-vacuum system with the valve closed and immersed in liquid nitrogen to freeze the sample. After roughly 2 h, when the sample was presumed to be frozen, the sample bottle was exposed to vacuum to remove any volatile impurities. After evacuating the vapor space, the sample cylinder valve was closed, detached from the vacuum system, and heated to drive the remaining volatile impurities into the vapor space. This process was repeated until the change in the vacuum gauge pressure was less than 10^{-2} Pa when exposing the vapor space

https://doi.org/10.1021/acs.jced.2c00037
J. Chem. Eng. Data 2022, 67, 1365−1377

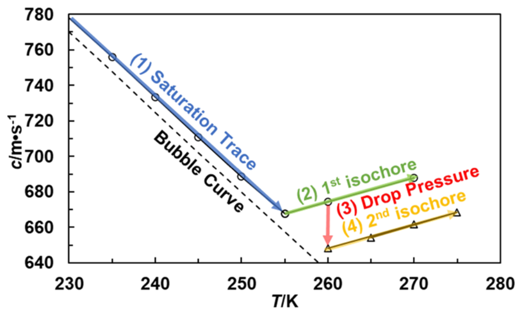

Figure 2. Isochoric speed of sound measurement sequence. (1) Initially, the measuring cell is full of liquid and the manifold contains vapor and the speed of sound data is measured at bubble point pressures intermediate to the measuring cell temperature and 293 K. (2) The measuring cell pressure surpasses the dew-point pressure at approximately 293 K; the manifold is full of liquid and measurements are carried out to a maximum pressure of 50 MPa. (3) Upon completion of the first isochore, the temperature is dropped to 5 K above the starting temperature, and the pressure is dropped to a condition 0.5 MPa above the bubble point pressure, and (4) measurements for the second isochore are initiated.

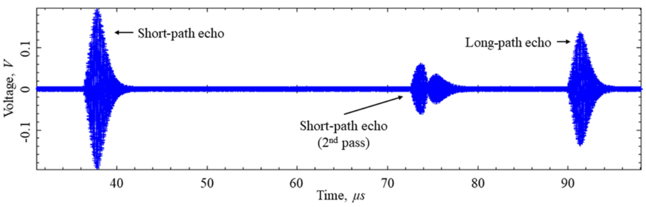

Figure 3. Typical oscilloscope trace for a speed of sound measurement encompassing 16,000 points inclusive of the first and second pass of the short-path echo and long-path echoes.

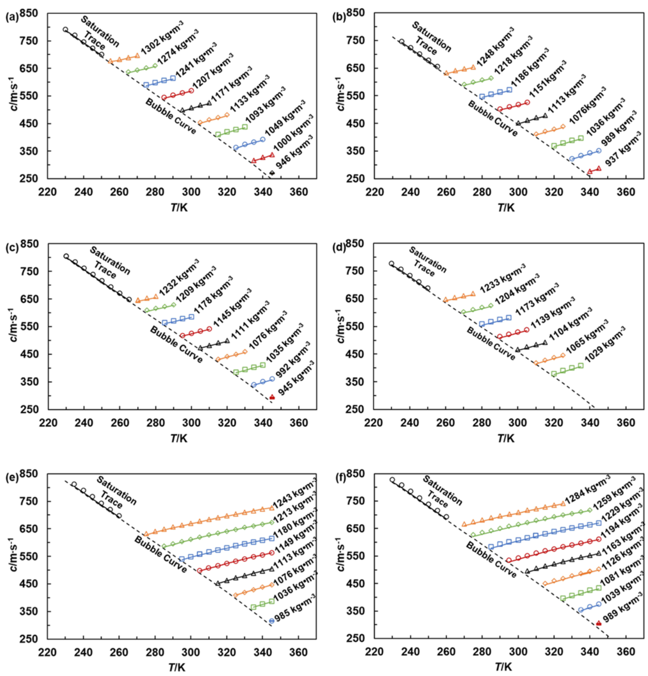

Figure 4. Relationship between the speed of sound, c, and temperature, T, for binary mixtures of R-134a, R-1234yf, and R-1234ze(E): (a) R-1234yf/134a (0.33634/0.66366), (b) R-1234yf/134a (0.66759/0.33241), (c) R-1234yf/1234ze(E) (0.33584/0.66416), (d) R-1234yf/1234ze(E) (0.66660/0.33340), (e) R-134a/1234ze(E) (0.32916/0.67084), and (f) R-134a/1234ze(E) (0.67102/0.32898) along several pseudo-isochores. Symbols represent experimental data points, while lines represent the speed of sound calculations using REFPROP for each pseudo-isochore.

to vacuum. Further details of the freeze−pump−thaw method are described by Outcalt and Rowane.[25]

Each mixture sample was prepared in the vapor phase, and the composition was determined gravimetrically using the double substitution method.[26] The double substitution method mitigates errors inherent to the balance used and accounts for the impact of air buoyancy on the sample cylinder. The standard deviation for each weighing was between 0.0006 and 0.0054 g, which translates into composition uncertainties between 5×10^{-6} and 4.4×10^{-5} mole fraction if only uncertainties associated with the gravimetric preparation are considered. However, additional sources of uncertainty may include contamination of the outside of the cylinder with dirt or moisture, expansion of the cylinder when filling, sorption of the sample onto the inner cylinder walls and valves as described by McLinden and Richter,[27] and loading uncertainties described in the next section. Nevertheless, including these additional sources of uncertainty, the overall composition uncertainty is no greater than 0.00010 mole fraction. Table 2 lists molar compositions, total sample volumes, and mole fraction uncertainties.

2.2. Dual-Path Pulse-Echo Instrument. The dual-path pulse-echo instrument is described in detail elsewhere by our group,[28,29] Ball and Trusler,[30] and Meier and Kabelac;[31] therefore, only the major features and details are described here. Figure 1 is a schematic diagram of the dual-path pulse-echo instrument showing the major components of the apparatus, which consists of a measurement cell contained within a pressure vessel that is housed in a precision thermostatted liquid bath (Fluke Hart Scientific, 7341 High Precision Bath) that can operate over the temperature range from 228 to 423 K. The measuring cell features a quartz crystal disk with a diameter of 24 mm, a thickness of 0.36 mm, and a resonant frequency of 8.00 MHz. The quartz crystal functions as an ultrasonic transducer and is "X-cut", so its thickness expands and contracts when a voltage is applied between electrodes on its opposing faces. Located between either face of the quartz crystal and reflectors on either end of the cell are two tubular ceramic spacers with lengths of approximately 12 and 30 mm that determine the length of the short and long echo paths, respectively. During an experiment, the quartz crystal functions as both a signal transmitter and receiver. The crystal is connected to a high-speed switch, which toggles its input between an arbitrary function generator (Agilent 33250A, 80 MHz) and a three-stage amplifier (Stanford Research Systems Inc., SR455A, 5× per stage for a total of 125×) that feeds into a digital storage oscilloscope (Keysight Infiniivision DSOX4022A, 200 MHz, 5 GSa/s). During a typical measurement sequence, the crystal is excited using the arbitrary function generator with a 10-cycle sinusoidal tone burst at 8 MHz, and then, after a 6 μs delay, the high-speed switch connects the crystal output to the three-stage amplifier and then to the digital storage oscilloscope. The echoes recorded by the oscilloscope are then analyzed off-line using the procedure described in the next section.

The pressure vessel is rated to 93 MPa and is configured with an electrical feedthrough from the top and tubing from the top and bottom of the vessel to the filling manifold (not pictured here). The filling manifold is also connected to a

https://doi.org/10.1021/acs.jced.2c00037
J. Chem. Eng. Data 2022, 67, 1365−1377

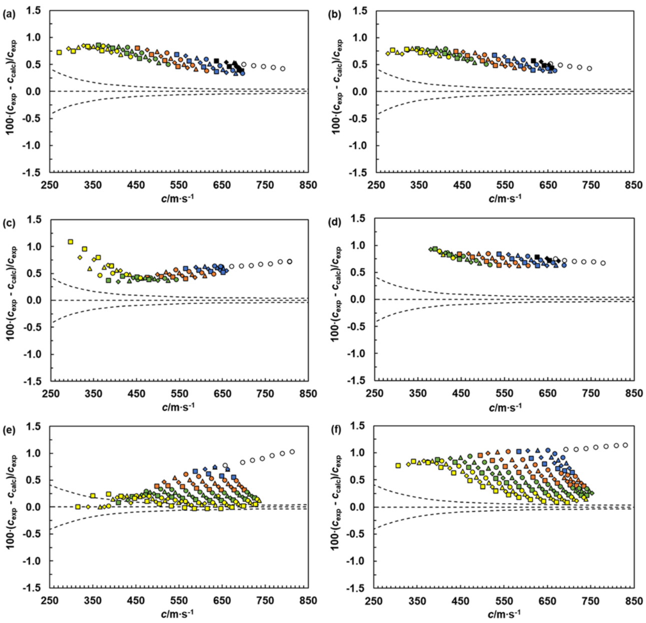

Figure 5. Deviaition graphs comparing the experimental speed of sound values, c_{exp}, to the speed of sound values calculated with REFPROP using the Helmholtz-energy-explicit EoS and binary interaction parameters reported by Bell et al.[8], c_{calc}, as a function of c_{exp}. Comparisons are for R-134a, R-1234yf, and R-1234ze(E) binary mixtures: (a) R-1234yf/134a (0.33634/0.66366), (b) R-1234yf/134a (0.66759/0.33241), (c) R-1234yf/1234ze(E) (0.33584/0.66416), (d) R-1234yf/1234ze(E) (0.66660/0.33340), (e) R-134a/1234ze(E) (0.32916/0.67084), and (f) R-134a/1234ze(E) (0.67102/0.32898) at temperatures open circle: tracing saturation, solid black triangle: 255 K, solid black diamond: 260 K, solid black square: 265 K, solid blue circle: 270 K, solid blue triangle: 275 K, solid blue diamond: 280 K, solid blue square: 285 K, solid orange circle: 290 K, :solid orange triangle: 295 K, solid orange diamond: 300 K, solid orange square: 305 K, solid green circle: 310 K, solid green triangle: 315 K, solid green diamond: 320 K, solid green square: 325 K, solid yellow circle: 330 K, solid yellow triangle: 335 K, solid yellow diamond: 340 K, and solid yellow square: 345 K.

vacuum system to evacuate the measuring cell and lines before loading new samples and a vibrating-quartz-crystal transducer (Paroscientific, Model# 420 K-HHT-101, 0−138 MPa) to measure the system pressure with a standard uncertainty of 0.014 MPa. Prior to loading the sample, the system is evacuated for at least 12 h to remove any residual sample from the previous run or solvent used to clean the system. As mentioned previously, the mixture samples are prepared in the vapor phase. Therefore, to ensure that the pressure vessel and measurement cell volumes are full of liquid, they must be cooled to a temperature at which the sample cylinder pressure exceeds the mixture dew-point pressure. The temperature of the pressure vessel and measurement cell is regulated using the liquid bath. The filling process is performed at 228 K to fill the pressure vessel with liquid.

As shown in Figure 1, filling lines from the top and the bottom of the pressure vessel extend from the filling manifold down into a bath. While filling the pressure vessel, the valves on the manifold are opened and closed in such a fashion that during the filling process, the vapor sample is forced through the bottom of the pressure vessel. Initially, the pressure vessel, the manifold, and filling lines are at vacuum pressure, while the sample cylinder pressure far exceeds both the bubble and dew-point pressures at 228 K. Initially, there is a possibility that the sample could fractionate as the sample begins to condense in the filling lines and pressure vessel. However, the system pressure quickly approaches the sample cylinder pressure forcing the sample to condense at the prepared sample composition. The entire filling process is given up to 2 h to fill the volumes of the system with liquid that are cooled to 228 K. Further, to confirm that no composition gradients remain and the sample is sufficiently remixed, the speed of sound is measured 12 times over a duration of 33 min and the standard deviation of these measurements was always well within the uncertainty of the speed of sound measurement. It is important to note that the manifold, which remains at room temperature, initially remains vapor-filled until the liquid expands to also fill the manifold.

Figure 2 demonstrates the isochoric measurement procedure for the speed of sound. The blue arrow in Figure 2 shows the measurements performed, while vapor resides in the manifold. As described previously, the system pressure is initially at bubble point pressures at temperatures intermediate to the cell temperature and 293 K. As the temperature of the system is increased, the fluid within the measurement cell expands and is pushed into the manifold. Eventually, once sufficient fluid is pushed into the manifold and the system pressure exceeds the dew-point pressure at T = 293 K, the vapor in the manifold begins to condense. Once all the vapor condenses to fill the manifold with liquid, the system enters the compressed-liquid region shown by the green arrow where increasing the temperature results in sharp pressure increases. In this study, data points along an isochore are taken in 5 K increments to a maximum pressure of 12 MPa for mixtures containing R-1234yf and 50 MPa for R-1234ze(E)/134a mixtures. Once the isochore is complete, the temperature is reduced to a condition 5 K above the starting temperature as shown by the red arrow. The pressure is then reduced by venting the sample to a condition 0.5 MPa above the bubble point estimated using REFPROP. This process is repeated until a data point just above the bubble point at 345 K is measured. In this study, our "isochores" are actually pseudo-isochores since the system volume varies slightly with changes in pressure and temperature due to the effect of compressibility and thermal expansion.

The bath temperature was measured with a 25 Ω reference standard platinum resistance thermometer (SPRT) located adjacent to the measuring cell. The resistance of the SPRT was ratioed with an AC resistance bridge to a standard resistor contained within a thermostatted enclosure. The SPRT, standard resistor, and resistance bridge system were calibrated with five ITS90 fixed point cells (mercury, water, indium, tin, and zinc) from 234.316 to 692.677 K. The standard uncertainty of the SPRT, standard resistor, and resistance bridge system was estimated to be 0.003 K. The experiment control was accomplished using a custom control program written in Visual Basic 6. The program performed a temperature and pressure scan of the system every 30 s, providing the information used to measure the system equilibration and stability. Three criteria were used to establish that the system was at equilibrium which are as follows: (1) the difference of the average of the previous eight temperature scans from the setpoint; (2) the standard deviation of the previous eight temperature scans; and (3) the rate of pressure change with time computed with a linear fit of the last eight pressure readings. When all three of the equilibrium criteria were within preset tolerances, a converged flag was set in the

Table 3. Experimental Speed of Sound Data for R-1234yf/134a Mixtures with a Molar Composition of (0.33634/0.66366)[a,b]

T/K	p/MPa	c/m s^{-1}	100·$U_c(c)$	T/K	p/MPa	c/m s^{-1}	100·$U_c(c)$	T/K	p/MPa	c/m s^{-1}	100·$U_c(c)$
230.013	0.353	790.84	0.04	279.999	4.586	599.13	0.06	320.004	8.941	481.25	0.08
235.007	0.658	769.59	0.04	285.000	7.981	606.95	0.05	309.997	1.503	431.03	0.11
240.004	0.678	746.67	0.04	290.003	11.378	614.61	0.05	314.994	3.859	440.71	0.10
245.004	0.690	723.74	0.04	279.998	0.890	565.36	0.06	320.004	6.236	450.01	0.09
250.005	0.704	700.89	0.05	285.000	4.124	573.74	0.06	325.009	8.608	458.78	0.09
254.995	1.231	682.11	0.05	290.003	7.359	581.87	0.06	314.992	1.733	409.82	0.12
259.987	5.247	689.09	0.05	294.998	10.590	589.77	0.05	320.002	3.960	419.66	0.11
264.996	9.178	695.40	0.04	284.998	1.183	545.28	0.07	325.008	6.201	429.07	0.10
254.993	0.651	677.79	0.05	290.001	4.259	553.65	0.06	330.000	8.441	437.99	0.09
259.986	4.420	683.24	0.05	294.997	7.347	561.90	0.06	320.002	1.827	386.04	0.14
264.996	8.392	690.07	0.04	299.998	10.440	569.91	0.06	325.008	3.924	396.35	0.13
269.993	12.399	697.15	0.04	290.000	1.199	522.32	0.07	330.000	6.023	405.99	0.11
259.986	1.278	659.86	0.05	294.997	4.134	531.05	0.07	335.004	8.112	414.85	0.11
264.995	5.122	666.92	0.05	299.999	7.087	539.59	0.06	325.006	2.025	363.70	0.16
269.993	9.068	674.67	0.05	304.998	10.041	547.87	0.06	329.999	3.980	374.21	0.14
274.996	12.964	681.96	0.04	294.996	1.213	499.13	0.08	335.002	5.935	383.73	0.13
264.994	1.260	637.06	0.05	299.998	4.004	508.17	0.07	340.007	7.905	392.88	0.12
269.991	4.977	644.66	0.05	304.998	6.801	516.85	0.07	329.998	2.229	341.01	0.19
274.995	8.710	652.21	0.05	310.000	9.603	525.24	0.07	335.002	4.041	351.53	0.17
279.999	12.442	659.66	0.05	299.997	1.313	476.73	0.09	340.007	5.877	361.47	0.15
269.991	1.167	613.65	0.05	304.996	3.957	485.96	0.08	345.013	7.718	370.79	0.13
274.995	4.716	621.41	0.05	309.999	6.613	494.84	0.08	335.001	2.392	317.01	0.23
280.000	8.276	629.11	0.05	314.995	9.266	503.35	0.07	340.006	4.087	328.15	0.20
285.001	11.853	636.78	0.05	304.995	1.397	453.89	0.10	345.013	5.792	338.36	0.17
274.993	1.193	591.14	0.06	309.998	3.908	463.47	0.09	340.006	2.607	293.45	0.28
				314.995	6.420	472.55	0.08	345.012	4.167	304.49	0.24
								345.012	2.910	271.59	0.34

[a]Listed are the temperature, T, pressure, P, speed of sound, c, and relative combined expanded uncertainty of the speed of sound, $U_c(c)$; speed of sound values listed are averaged from up to 12 measurements at each state point. [b]The combined expanded uncertainty of the composition is $U_c(x_1)$ = 0.00010 mole fraction, and the standard uncertainties for temperature and pressure are $u_c(T)$ = 0.004 K and $u_c(p)$ = 0.014 MPa, respectively. Expanded uncertainties are specified with a coverage factor, k = 2.

control program. After an additional 30 min equilibration time, the speed of sound measurements were initiated. At each state point investigated, 12 replicate speeds of sound measurements were performed. The short-term temperature fluctuations (minute-to-minute) were 0.002 K with negligible long-term temperature variations. Temperature gradients in the oil bath surrounding the pressure vessel were less than 0.0025 K, resulting in a combined standard uncertainty for the entire system of 0.004 K.

2.3. Measurement Principle. The speed of sound measurement is initiated by exciting a piezoelectric element (in this case, an X-cut quartz crystal) with an arbitrary function generator to generate a tone burst at its resonant frequency. The tone burst traverses the fluid in two different directions along short and long paths and returns from the flat reflectors. The quartz crystal is switched from the "transmit" mode to the "receive mode" to record the echoes from both the short and long paths. Figure 3 shows the voltage recorded from the oscilloscope as a function of time for a single pulse-echo event. The data shown in Figure 3 encompasses 16,000 data points, which includes the first and second passes for the short-path echo and the long-path echo. The speed of sound, c, is determined from the relationship

$$c = \frac{2(L_{\text{long}} - L_{\text{short}})}{\Delta t} \tag{1}$$

where L_{long} and L_{short} are the distances of the short and long paths, respectively, and Δt is the time delay between the arrival of the short-path and long-path echoes. As described in a previous study,[28,29] the quantity ($L_{\text{long}} - L_{\text{short}}$) is determined as a function of temperature and pressure by calibration with a reference fluid, which in this case was liquid propane. Notice in Figure 3 that the short- and long-path echoes exhibit virtually the same shape with different amplitudes. The amplitude of the long-path echo is damped in comparison to the short path due to the greater degree of attenuation encountered. Therefore, with a scaling factor for the amplitude, the short- and long-path echoes can be superimposed. The initial guess for Δt is determined by finding the maximum amplitude for both echoes and is then optimized using linear regression. Also included in the data analysis is a diffraction correction which accounts for phase advance as the sound wave propagates through the fluid. A more in-depth explanation describing the method used here to determine Δt and the diffraction correction is described elsewhere.[29]

2.4. Measurement Uncertainty. Eq 2 was used to estimate the relative combined expanded uncertainty of the speed of sound measurement.

$$\frac{U_c(c)}{\%} = 2 \times 100 \times \frac{1}{c}\sqrt{\left\{u^2(c) + \left[\frac{\partial c}{\partial T}\right]^2 u^2(T) + \left[\frac{\partial c}{\partial p}\right]^2 u^2(p) + \left[\frac{\partial c}{\partial x_i}\right]^2 u^2(x_i)\right\}} \tag{2}$$

The "2" on the right-hand side of the equation represents a coverage factor of k = 2 needed to obtain an expanded

https://doi.org/10.1021/acs.jced.2c00037
J. Chem. Eng. Data 2022, 67, 1365−1377

Table 4. Experimental Speed of Sound Data for the R-1234yf/134a Mixture with a Molar Composition of (0.66759/0.33241)[a,b]

T/K	p/MPa	c/m s^{-1}	100·$U_c(c)$	T/K	p/MPa	c/m s^{-1}	100·$U_c(c)$	T/K	p/MPa	c/m s^{-1}	100·$U_c(c)$	T/K	p/MPa	c/m s^{-1}	100·$U_c(c)$
235.007	0.663	746.03	0.04	285.001	11.008	614.44	0.05	299.998	3.860	489.10	0.08	329.999	7.794	418.17	0.10
240.002	0.672	723.28	0.04	274.994	1.218	570.34	0.06	304.998	6.446	497.61	0.08	320.001	1.869	369.14	0.16
245.003	0.694	700.73	0.05	279.999	4.366	578.19	0.06	309.999	9.038	505.86	0.07	325.008	3.802	379.36	0.14
250.004	0.708	678.16	0.05	285.001	7.517	585.89	0.06	299.996	0.972	452.68	0.10	330.000	5.728	388.77	0.13
254.995	0.720	655.72	0.05	290.002	10.656	593.38	0.05	304.996	3.395	461.90	0.09	335.006	7.635	397.31	0.12
259.987	2.996	651.70	0.05	279.998	1.243	548.15	0.07	309.999	5.829	470.77	0.08	325.006	1.989	345.81	0.18
264.997	6.626	658.38	0.05	284.999	4.239	556.18	0.06	314.994	8.257	479.23	0.08	329.998	3.782	356.19	0.16
269.993	10.288	665.31	0.05	290.003	7.244	564.05	0.06	304.995	1.420	435.21	0.11	335.003	5.578	365.68	0.14
260.001	0.801	633.95	0.05	294.998	10.251	571.77	0.06	309.998	3.733	444.58	0.10	340.008	7.384	374.72	0.13
264.995	4.338	640.85	0.05	284.998	1.205	525.15	0.07	314.994	6.045	453.48	0.09	329.998	2.169	323.07	0.22
269.993	7.925	648.05	0.05	290.002	4.071	533.56	0.07	320.004	8.354	461.92	0.08	335.003	3.829	333.61	0.19
274.995	11.487	654.98	0.05	294.998	6.933	541.67	0.06	309.996	1.406	411.00	0.12	340.008	5.503	343.40	0.17
264.994	1.250	615.38	0.05	299.998	9.802	549.61	0.06	314.994	3.578	420.69	0.11	345.013	7.185	352.57	0.15
269.992	4.705	622.85	0.05	290.000	1.169	501.82	0.08	320.003	5.762	429.89	0.10	335.001	2.323	299.00	0.27
274.995	8.164	630.22	0.05	294.997	3.881	510.45	0.07	325.009	7.944	438.60	0.09	340.004	3.868	309.86	0.23
280.000	11.622	637.48	0.05	299.999	6.601	518.81	0.07	314.992	1.632	390.16	0.14	345.013	5.424	320.37	0.20
269.990	1.132	591.90	0.06	304.997	9.317	526.84	0.07	320.001	3.686	400.08	0.12	340.005	2.580	277.01	0.33
274.995	4.413	599.48	0.06	294.995	1.281	480.27	0.09	325.008	5.741	409.38	0.11	345.013	3.999	288.20	0.27
279.999	7.714	607.04	0.05												

[a]Listed are the temperature, T, pressure, P, speed of sound, c, and relative combined expanded uncertainty of the speed of sound, $U_c(c)$. Speed of sound values listed are averaged from up to 12 measurements at each state point. [b]The combined expanded uncertainty of the composition is $U_c(x_1) = 0.00010$ mole fraction, and the standard uncertainties for temperature and pressure are $u_c(T) = 0.004$ K and $u_c(p) = 0.014$ MPa, respectively. Expanded uncertainties are specified with a coverage factor, $k = 2$.

https://doi.org/10.1021/acs.jced.2c00037
J. Chem. Eng. Data 2022, 67, 1365−1377

Table 5. Experimental Speed of Sound Data for the R-1234yf/1234ze(E) Mixture with a Molar Composition of (0.33584/0.66416)[a,b]

T/K	p/MPa	c/m s^{-1}	100·$U_c(c)$	T/K	p/MPa	c/m·s^{-1}	100·$U_c(c)$	T/K	p/MPa	c/m·s^{-1}	100·$U_c(c)$	T/K	p/MPa	c/m·s^{-1}	100·$U_c(c)$
229.999	0.263	806.07	0.04	274.993	1.131	609.30	0.06	304.996	6.527	534.46	0.07	320.001	1.562	407.47	0.13
230.014	0.267	806.10	0.04	279.998	4.419	616.37	0.05	309.999	9.236	541.90	0.06	325.007	3.651	416.91	0.12
235.008	0.521	784.77	0.04	285.000	7.667	623.04	0.05	299.996	1.352	498.92	0.08	329.999	5.740	425.83	0.11
240.003	0.542	761.96	0.04	290.002	10.969	630.08	0.05	304.996	3.965	507.27	0.08	335.003	7.817	434.09	0.10
245.003	0.534	739.27	0.04	279.997	1.194	587.52	0.06	309.999	6.596	515.51	0.07	325.006	1.684	384.70	0.15
250.004	0.543	716.62	0.04	285.000	4.323	594.65	0.06	314.994	9.206	523.32	0.07	329.998	3.647	394.49	0.13
254.995	0.542	694.03	0.05	290.002	7.458	601.75	0.05	304.994	1.235	474.32	0.09	335.003	5.598	403.39	0.12
259.987	0.551	671.60	0.05	294.998	10.584	608.69	0.05	309.998	3.713	483.04	0.08	340.007	7.566	412.01	0.11
264.995	0.547	649.01	0.05	284.999	1.104	564.22	0.06	314.994	6.188	491.40	0.08	329.998	1.945	364.29	0.17
269.992	2.854	645.90	0.05	290.001	4.108	571.77	0.06	320.003	8.666	499.42	0.07	335.002	3.785	374.11	0.15
269.991	2.931	646.50	0.05	294.997	7.105	579.14	0.06	309.997	1.379	452.78	0.10	340.007	5.635	383.35	0.13
274.995	6.403	652.94	0.05	299.999	10.097	586.32	0.06	314.993	3.723	461.69	0.09	345.013	7.491	392.12	0.12
279.999	9.895	659.50	0.05	290.000	1.075	541.34	0.07	320.004	6.073	470.18	0.09	335.001	2.049	340.38	0.20
269.991	1.097	631.33	0.05	294.997	3.934	549.11	0.07	325.009	8.419	478.31	0.08	340.006	3.780	350.84	0.17
274.994	4.515	638.06	0.05	299.999	6.792	556.67	0.06	314.992	1.642	432.89	0.11	345.012	5.516	360.52	0.16
279.999	7.939	644.80	0.05	304.997	9.651	564.09	0.06	320.002	3.877	442.08	0.10	340.006	2.260	318.25	0.23
285.000	11.337	651.32	0.05	294.995	1.063	518.44	0.08	325.008	6.112	450.77	0.09	345.012	3.869	328.91	0.20
				299.998	3.801	526.62	0.07	329.999	8.337	459.02	0.09	345.012	2.476	295.80	0.29

[a]Listed are the temperature, T, pressure, P, speed of sound, c, and relative combined expanded uncertainty of the speed of sound, $U_c(c)$; speed of sound values listed are averaged from up to 12 measurements at each state point. [b]The combined expanded uncertainty of the composition is $U_c(x_1) = 0.00010$ mole fraction, and the standard uncertainties for temperature and pressure are $u_c(T) = 0.004$ K and $u_c(p) = 0.014$ MPa, respectively. Expanded uncertainties are specified with a coverage factor, $k = 2$.

https://doi.org/10.1021/acs.jced.2c00037
J. Chem. Eng. Data 2022, 67, 1365−1377

Table 6. Experimental Speed of Sound Data for the R-1234yf /1234ze(E) Mixture with a Molar Composition of (0.66660/0.33340)[a,b]

T/K	p/MPa	c/m s^{-1}	100·$U_c(c)$	T/K	p/MPa	c/m s^{-1}	100·$U_c(c)$	T/K	p/MPa	c/m s^{-1}	100·$U_c(c)$
229.998	0.450	777.99	0.04	274.993	1.123	581.33	0.06	299.996	1.030	467.14	0.09
235.008	0.591	756.13	0.04	279.999	4.282	589.10	0.06	304.996	3.494	476.27	0.09
240.004	0.607	733.50	0.04	285.000	7.446	596.77	0.06	310.000	5.961	485.01	0.08
245.003	0.616	710.97	0.04	290.002	10.608	604.28	0.05	314.993	8.401	493.16	0.08
250.005	0.624	688.51	0.05	279.997	1.130	559.12	0.06	304.995	1.196	446.00	0.10
254.994	0.792	667.55	0.05	285.000	4.140	567.06	0.06	309.998	3.530	455.33	0.09
259.987	4.524	674.41	0.05	290.003	7.161	574.92	0.06	314.994	5.869	464.26	0.09
269.993	11.961	687.78	0.04	294.997	10.166	582.50	0.06	320.004	8.211	472.78	0.08
259.986	1.160	648.25	0.05	284.999	1.148	536.92	0.07	309.997	0.984	418.91	0.12
265.003	4.628	654.24	0.05	290.001	4.005	545.01	0.07	314.993	3.165	428.60	0.11
269.990	8.269	661.67	0.05	294.998	6.873	552.95	0.06	320.005	5.351	437.71	0.10
274.995	11.836	668.41	0.05	299.999	9.747	560.75	0.06	325.008	7.532	446.32	0.09
264.994	1.127	625.75	0.05	290.000	1.030	513.07	0.08	314.991	1.535	403.52	0.13
269.991	4.572	633.05	0.05	294.997	3.758	521.57	0.07	320.002	3.623	413.31	0.12
274.995	8.070	640.62	0.05	299.998	6.487	529.78	0.07	325.008	5.715	422.57	0.11
280.000	11.531	647.83	0.05	304.998	9.212	537.70	0.06	329.999	7.793	431.19	0.10
269.991	1.128	603.60	0.06	294.995	1.070	490.76	0.08	320.002	1.614	380.30	0.15
274.994	4.428	611.11	0.05	299.998	3.690	499.76	0.08	325.008	3.572	390.39	0.13
280.000	7.740	618.59	0.05	304.997	6.300	508.33	0.07	329.999	5.527	399.80	0.12
285.001	11.049	625.95	0.05	309.998	8.904	516.52	0.07	335.004	7.472	408.44	0.11

[a]Listed are the temperature, T, pressure, P, speed of sound, c, and relative combined expanded uncertainty of the speed of sound, $U_c(c)$; speed of sound values listed are averaged from up to 12 measurements at each state point. [b]The combined expanded uncertainty of the composition is $U_c(x_1)$ = 0.00010 mole fraction, and the standard uncertainties for temperature and pressure are $u_c(T)$ = 0.004 K and $u_c(p)$ = 0.014 MPa, respectively. Expanded uncertainties are specified with a coverage factor, k = 2.

uncertainty with a 95.45% confidence interval. The standard uncertainty of the speed of sound, temperature, and pressure is determined from the standard deviation of up to 12 measurements and systematic uncertainties (0.004 K, 0.014 MPa, and 0.00010 mole fraction). The partial derivative terms capturing the sensitivity of the speed of sound with respect to temperature, pressure, and composition were estimated using the Helmholtz-energy-explicit EoS[21−24] embedded in REFPROP.[20] The $u^2(c)$ term is inclusive of uncertainties attributed to the calibration of the instrument path length and further contributions associated with temperature, pressure, and the time delay between short- and long-path echo arrivals. The relative combined expanded uncertainty of the measurement is determined at each individual state point since it varies significantly with the magnitude of the speed of sound. As the system approached the mixture critical region, lower speed of sound values and weaker echo signals were encountered, which increased the uncertainty in Δt. The oscilloscope recorded 16,000 data points from the start of the short-path echo to the end of the long-path echo including the time between the echoes. The decrease in the speed of sound results in a greater distance between the short- and long-path echo signals, which reduces the number of data points that can be superimposed to determine Δt. Consequently, this reduced number of data points increases the relative combined expanded uncertainty in c. Weaker echo signals also contribute to greater uncertainties in c due to a larger signal to noise ratio encountered when determining Δt. This greater signal to noise ratio increases the variance in the regression procedure since the echo signals cannot be exactly superimposed cycle for cycle.

3. EXPERIMENTAL RESULTS

3.1. Measured Data. Figure 4a−f shows the relationship between the speed of sound and temperature for several pseudo-isochores and several T-c points near saturation for binary refrigerant mixtures. Only select isochores are depicted in Figure 4a−f to reduce clutter on the plots. Densties calculated using REFPROP show that for a given pseudo-isochore, the densities do not vary by more than 10 kg m^{-3}. Lines drawn on the plots in Figure 4a−f are REFPROP[20] calculations using available Helmholtz-energy-explicit EoS for R-1234yf,[22] R-134a,[21] and R-1234ze(E)[23] and independently reported binary interaction parameters[8] for each binary mixture. It is important to note that the EoS used in this study developed by Lemmon and Akasaka is not included in REFPROP version 10.0 which by default uses the EoS of Richter et al.[18] In this study, the REFPROP models were used for comparison, and no adjustments were made to the binary interaction parameters. Tables 3−8 list the pressure, temperature, speed of sound, and relative combined expanded uncertainty of the speed of sound for the averaged speed of sound measurements. As mentioned in the previous section, up to 12 measurements were taken at each state point to quantify the reproducibility and uncertainy of the technique. Data files containing the raw unaveraged data are available in the Supporting Information and are also deposited at data.nist.gov.[32]

3.2. Comparison with REFPROP Models. Figure 5a−f shows deviation graphs comparing the speed of sound data reported in this study to the current REFPROP mixture models. Dashed lines in each figure are smoothed curves of the relative combined expanded experimental uncertainty of each measurement, which as described previously increases as the magnitude of the speed of sound decreases. The overall comparison of the data from the present study to the current

Table 7. Experimental Speed of Sound Data for the R-134a/1234ze(E) Mixture with a Molar Composition of (0.32916/0.67084)[a,b]

T/K	p/MPa	c/m s^{-1}	100·$U_c(c)$	T/K	p/MPa	c/m·s^{-1}	100·$U_c(c)$	T/K	p/MPa	c/m·s^{-1}	100·$U_c(c)$	T/K	p/MPa	c/m·s^{-1}	100·$U_c(c)$
235.008	0.525	812.57	0.04	279.994	0.983	610.28	0.06	329.999	26.574	628.01	0.05	314.989	3.848	482.89	0.08
240.003	0.537	789.62	0.04	284.996	4.446	618.17	0.05	335.003	29.665	634.47	0.04	320.000	6.456	492.03	0.08
245.004	0.541	766.62	0.04	289.998	7.896	625.79	0.05	340.006	32.755	640.89	0.04	325.006	9.061	500.75	0.07
250.004	0.549	743.64	0.04	294.994	11.388	633.58	0.05	345.014	35.827	647.15	0.04	329.997	11.654	509.07	0.07
254.994	0.553	720.81	0.04	299.996	14.861	641.10	0.05	294.991	0.899	540.26	0.07	335.002	14.232	516.91	0.07
259.987	0.559	698.02	0.05	304.995	18.318	648.38	0.05	299.994	3.918	549.04	0.07	340.007	16.806	524.47	0.06
269.992	1.140	657.06	0.05	309.997	21.756	655.44	0.04	304.993	6.942	557.56	0.06	345.012	19.379	531.84	0.06
274.995	4.782	663.40	0.05	314.993	25.181	662.33	0.04	309.996	9.974	565.85	0.06	314.990	1.546	453.04	0.10
280.000	8.458	669.98	0.05	320.003	28.593	669.03	0.04	314.991	12.986	573.78	0.06	319.999	4.024	462.90	0.09
285.001	12.144	676.62	0.04	325.009	31.978	675.51	0.04	320.001	15.983	581.33	0.05	325.005	6.490	472.10	0.08
290.003	15.823	683.20	0.04	330.000	35.346	681.89	0.04	325.007	18.972	588.66	0.05	329.997	8.953	480.84	0.08
294.998	19.487	689.68	0.04	335.003	38.647	687.82	0.04	329.999	21.942	595.75	0.05	335.002	11.402	489.00	0.07
299.999	23.144	696.07	0.04	340.008	41.950	693.72	0.04	335.003	24.877	602.46	0.05	340.008	13.858	496.96	0.07
304.997	26.739	702.09	0.04	345.012	45.243	699.54	0.04	340.007	27.825	609.15	0.05	345.013	16.312	504.64	0.07
310.000	30.316	707.98	0.04	284.995	1.030	587.84	0.06	345.013	30.764	615.69	0.05	319.999	1.756	431.60	0.11
314.994	33.894	713.91	0.04	289.997	4.364	596.15	0.06	299.991	0.756	515.11	0.08	325.005	4.078	441.42	0.10
320.004	37.460	719.74	0.04	294.994	7.702	604.29	0.05	304.993	3.626	524.27	0.07	329.997	6.412	450.80	0.09
325.010	41.009	725.47	0.04	299.996	11.081	612.50	0.05	309.995	6.506	533.14	0.07	335.001	8.742	459.60	0.09
330.000	44.515	731.03	0.04	304.995	14.423	620.29	0.05	314.991	9.373	541.58	0.06	340.007	11.076	468.04	0.08
335.004	47.984	736.38	0.04	309.997	17.750	627.78	0.05	320.001	12.244	549.72	0.06	345.013	13.404	476.10	0.08
340.009	51.440	741.68	0.04	314.992	21.047	634.96	0.05	325.007	15.100	557.52	0.06	325.005	1.948	409.78	0.12
274.989	1.010	633.32	0.05	320.001	24.301	641.73	0.05	329.998	17.941	565.04	0.05	329.997	4.146	419.95	0.11
279.995	4.674	641.29	0.05	325.008	27.528	648.23	0.04	335.002	20.767	572.22	0.05	335.001	6.350	429.46	0.10
284.997	8.321	649.02	0.05	329.999	30.759	654.73	0.04	340.008	23.590	579.25	0.05	340.007	8.553	438.42	0.10
290.000	11.947	656.43	0.05	335.003	33.970	661.02	0.04	345.013	26.400	586.06	0.05	345.012	10.760	446.98	0.09
294.995	15.574	663.80	0.05	340.008	37.171	667.20	0.04	304.991	1.377	498.72	0.08	329.998	2.044	386.06	0.14
299.996	19.173	670.85	0.04	345.013	40.356	673.25	0.04	309.994	4.125	507.93	0.08	335.002	4.096	396.26	0.13
304.995	22.769	677.82	0.04	289.996	1.161	566.13	0.06	314.990	6.876	516.79	0.07	340.006	6.157	405.92	0.12
309.998	26.350	684.61	0.04	294.992	4.345	574.65	0.06	320.001	9.632	525.29	0.07	345.013	8.225	415.07	0.11
314.993	29.899	691.17	0.04	299.994	7.543	583.01	0.06	325.007	12.380	533.43	0.06	335.000	2.385	366.39	0.16
320.005	33.452	697.64	0.04	304.994	10.731	591.05	0.05	329.998	15.115	541.25	0.06	340.006	4.329	377.01	0.14
325.008	36.980	703.96	0.04	309.996	13.911	598.82	0.05	335.003	17.824	548.60	0.06	345.013	6.278	386.87	0.13
329.999	40.468	710.07	0.04	314.992	17.077	606.34	0.05	340.008	20.519	555.69	0.06	340.005	2.348	338.90	0.20
335.004	43.903	715.84	0.04	320.003	20.248	613.69	0.05	345.013	23.229	562.73	0.05	345.013	4.140	349.93	0.17
340.008	47.327	721.56	0.04	325.008	23.442	621.11	0.05	309.993	1.253	473.32	0.09	345.010	2.550	315.54	0.24
345.014	50.738	727.19	0.04												

[a]Listed are the temperature, T, pressure, P, speed of sound, c, and relative combined expanded uncertainty of the speed of sound, $U_c(c)$; speed of sound values listed are averaged from up to 12 measurements at each state point. [b]The combined expanded uncertainty of the composition is $U_c(x_1) = 0.00010$ mole fraction, and the standard uncertainties for temperature and pressure are $u_c(T) = 0.004$ K and $u_c(p) = 0.014$ MPa, respectively. Expanded uncertainties are specified with a coverage factor, $k = 2$.

https://doi.org/10.1021/acs.jced.2c00037
J. Chem. Eng. Data 2022, 67, 1365−1377

Table 8. Experimental Speed of Sound Data for R-134a/1234ze(E) Mixtures with a Molar Composition of (0.67102/0.32898)[a,b]

T/K	p/MPa	c/m s^{-1}	$100 \cdot U_c(c)$	T/K	p/MPa	c/m s^{-1}	$100 \cdot U_c(c)$	T/K	p/MPa	c/m s^{-1}	$100 \cdot U_c(c)$	T/K	p/MPa	c/m s^{-1}	$100 \cdot U_c(c)$
229.997	0.131	829.10	0.04	320.004	39.328	721.55	0.04	330.000	31.643	651.94	0.04	325.007	13.007	530.95	0.06
235.007	0.589	808.34	0.04	325.009	43.044	727.69	0.04	335.003	34.896	658.15	0.04	329.998	15.788	538.80	0.06
240.004	0.609	785.19	0.04	330.000	46.700	733.54	0.04	340.009	38.152	664.32	0.04	335.002	18.543	546.15	0.06
245.006	0.605	761.97	0.04	335.004	50.316	739.13	0.04	345.013	41.393	670.37	0.04	340.008	21.304	553.38	0.05
250.005	0.609	738.83	0.04	274.990	1.038	627.36	0.05	289.996	1.173	559.27	0.07	345.013	24.059	560.42	0.05
254.994	0.618	715.85	0.04	279.995	4.733	635.34	0.05	294.993	4.392	567.96	0.06	309.994	1.809	472.09	0.09
259.988	0.611	692.86	0.05	284.997	8.434	643.22	0.05	299.994	7.623	576.43	0.06	314.990	4.450	481.66	0.08
269.993	5.812	685.99	0.05	290.000	12.131	650.91	0.05	304.994	10.850	584.61	0.06	320.002	7.105	490.82	0.08
274.995	9.842	693.24	0.04	294.995	15.817	658.41	0.05	309.996	14.070	592.50	0.05	325.006	9.758	499.55	0.07
280.000	13.884	700.47	0.04	299.997	19.484	665.63	0.04	314.993	17.273	600.08	0.05	329.999	12.400	507.86	0.07
285.001	17.913	707.56	0.04	304.995	23.137	672.69	0.04	320.002	20.478	607.48	0.05	335.003	15.021	515.63	0.06
290.003	21.919	714.46	0.04	309.998	26.772	679.54	0.04	325.008	23.661	614.60	0.05	340.007	17.643	523.20	0.06
294.998	25.905	721.19	0.04	314.994	30.385	686.21	0.04	330.000	26.822	621.49	0.05	345.013	20.252	530.47	0.06
299.999	29.876	727.77	0.04	320.004	33.986	692.71	0.04	335.002	29.939	627.95	0.04	314.990	1.964	449.98	0.10
304.998	33.823	734.20	0.04	325.009	37.562	699.04	0.04	340.007	33.106	634.64	0.04	319.999	4.471	459.83	0.09
310.000	37.736	740.43	0.04	330.000	41.101	705.15	0.04	345.012	36.236	641.04	0.04	325.006	6.981	469.12	0.09
314.995	41.622	746.51	0.04	335.003	44.595	710.97	0.04	294.991	1.056	534.63	0.07	329.998	9.484	477.92	0.08
320.004	45.494	752.47	0.04	340.007	48.088	716.76	0.04	299.994	4.110	543.54	0.07	335.003	11.973	486.12	0.07
269.993	3.174	666.80	0.05	279.994	1.100	604.88	0.06	304.993	7.173	552.18	0.06	340.007	14.470	494.12	0.07
274.995	7.130	674.44	0.05	284.996	4.633	613.08	0.05	309.996	10.239	560.54	0.06	345.013	16.965	501.84	0.07
280.000	11.085	681.95	0.04	289.999	8.175	621.14	0.05	314.991	13.297	568.59	0.06	319.999	2.064	426.84	0.11
285.001	15.028	689.29	0.04	294.995	11.707	628.97	0.05	320.003	16.348	576.32	0.05	325.006	4.432	436.97	0.10
290.003	18.959	696.46	0.04	299.996	15.229	636.54	0.05	325.008	19.388	583.79	0.05	329.997	6.793	446.45	0.09
294.999	22.863	703.42	0.04	304.996	18.740	643.90	0.05	329.997	22.381	590.80	0.05	335.002	9.139	455.13	0.09
299.999	26.745	710.16	0.04	309.997	22.215	650.90	0.04	335.002	25.368	597.59	0.05	340.007	11.502	463.64	0.08
304.998	30.611	716.76	0.04	314.994	25.689	657.82	0.04	340.009	28.359	604.32	0.05	345.013	13.861	471.75	0.08
310.000	34.457	723.21	0.04	320.003	29.154	664.55	0.04	345.012	31.341	610.89	0.05	325.004	1.764	396.62	0.14
314.993	38.265	729.45	0.04	325.009	32.599	671.10	0.04	299.992	1.274	513.38	0.08	329.997	3.937	406.94	0.12
320.004	42.025	735.38	0.04	330.000	36.014	677.47	0.04	304.992	4.193	522.57	0.07	335.002	6.104	416.39	0.11
325.008	45.773	741.24	0.04	335.004	39.380	683.47	0.04	309.995	7.123	531.46	0.07	340.007	8.292	425.54	0.10
269.987	1.099	650.78	0.05	340.008	42.752	689.47	0.04	314.992	10.048	539.99	0.06	345.013	10.485	434.26	0.09
274.991	4.970	658.61	0.05	345.013	46.114	695.38	0.04	320.001	12.974	548.17	0.06	329.996	2.021	374.75	0.16
279.996	8.848	666.34	0.05	284.995	1.402	584.62	0.06	325.007	15.890	556.02	0.06	335.001	4.057	385.21	0.14
284.998	12.716	673.89	0.04	289.997	4.794	593.04	0.06	329.999	18.784	563.55	0.05	340.007	6.114	395.14	0.12
290.001	16.573	681.26	0.04	294.995	8.187	601.25	0.05	335.002	21.654	570.67	0.05	345.013	8.179	404.50	0.11
294.996	20.399	688.35	0.04	299.996	11.580	609.23	0.05	340.007	24.524	577.65	0.05	335.001	2.355	354.21	0.18
299.998	24.212	695.26	0.04	304.994	14.949	616.85	0.05	345.013	27.388	584.46	0.05	340.007	4.283	365.13	0.16
304.997	28.005	702.00	0.04	309.997	18.320	624.30	0.05	304.992	1.802	495.84	0.08	345.013	6.220	375.25	0.14
309.999	31.782	708.59	0.04	314.992	21.683	631.61	0.05	309.995	4.602	505.21	0.08	340.007	2.528	330.08	0.21
314.996	35.538	715.02	0.04	320.002	25.028	638.61	0.05	314.990	7.403	514.17	0.07	345.012	4.316	341.30	0.18
				325.009	28.354	645.41	0.04	320.001	10.211	522.77	0.07	345.013	2.760	306.71	0.25

https://doi.org/10.1021/acs.jced.2c00037
J. Chem. Eng. Data 2022, 67, 1365−1377

Table 8. continued

[a] Listed are the temperature, T, pressure, P, speed of sound, c, and relative combined expanded uncertainty of the speed of sound, $U_c(c)$; speed of sound values listed are averaged from up to 12 measurements at each state point. [b] The combined expanded uncertainty of the composition is $U_c(x_1) = 0.00010$ mole fraction, and the standard uncertainties for temperature and pressure are $u_c(T) = 0.004$ K and $u_c(p) = 0.014$ MPa, respectively. Expanded uncertainties are specified with a coverage factor, $k = 2$.

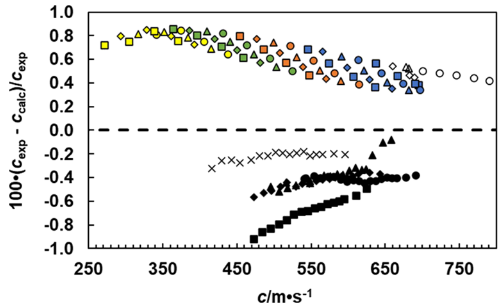

Figure 6. Comparison of the R-1234yf/134a mixture with a molar composition of (0.33634/0.66366). Speed of sound data reported in this study at temperatures: open circle: tracing saturation, open triangle: 255 K, open diamond: 260 K, open square: 265 K, solid blue circle: 270 K, solid blue triangle: 275 K, solid blue diamond: 280 K, solid blue square: 285 K, solid orange circle: 290 K, solid orange triangle: 295 K, solid orange diamond: 300 K, solid orange square: 305 K, solid green circle: 310 K, solid green triangle 315 K, solid green diamond: 320 K, solid green square: 325 K, open yellow circle: 330 K, open yellow triangle: 335 K, open yellow diamond: 340 K, and open yellow square: 345 K, and comparison of R-1234yf/134a (0.3736/0.6264) speed of sound data of Shimoura et al. at temperatures:solid black circle: 283, solid black triangle: 293, solid black diamond: 298, solid black square: 303, and black x: 313 K, c_{exp}, to the speed of sound calculations using REFPROP, c_{calc}.

REFPROP Helmholtz-energy-explicit EoS is characterized using the average absolute deviation, Δ_{AAD}, given by eq 3. The Δ_{AAD} values range from 0.27 to 0.75% for the six mixtures studied here. Additionally, when comparing REFPROP to all six mixtures, the maximum deviation, $\Delta_{\max}$, given by eq 4 is 1.12%. The quantity $c_{i,\text{exp}}$ is an experimental speed of sound data point, $c_{i,\text{calc}}$ is a speed of sound value calculated using REFPROP, and N is the number of data points. Positive systematic deviations are seen for all six mixtures studied. The deviation graphs in Figure 5a−f show that the REFPROP models underpredict the speed of sound for all six mixtures. It is important to reiterate that no adjustments were made to the REFPROP Helmholtz-energy-explicit EoS using the data reported in the present study. Therefore, in further studies, the data reported here will be used to improve the R-134a/1234yf, R-1234yf/1234ze(E), and R-134a/1234ze(E) mixture EoS.

$$\Delta_{\text{AAD}} = 100 \cdot \frac{1}{N} \sum_{i=0}^{N} \left| \frac{c_{i,\text{exp}} - c_{i,\text{calc}}}{c_{i,\text{exp}}} \right| \tag{3}$$

$$\Delta_{\max} = \max\left(100 \cdot \left| \frac{c_{i,\text{exp}} - c_{i,\text{calc}}}{c_{i,\text{exp}}} \right|\right) \tag{4}$$

The data of Shimoura et al.[17] is the only literature data set that allows for a meaningful comparison to the data obtained in this study. However, Shimoura et al. only report R-1234yf/134a mixture data at a single composition of (0.3736/0.6264) mole fraction from 283 to 313 K up to a pressure of 20 MPa. Figure 6 is a deviation plot comparing the R-1234yf/134a (0.33634/0.66366) mole fraction data reported in this study and the R-1234yf/134a (0.3736/0.6264) mole fraction data reported by Shimoura et al. to the Helmholtz-energy-explicit EoS included in REFPROP. The speed of sound data reported in the present study exhibits only positive deviations from the REFPROP EoS consistent with the other five mixtures studied

https://doi.org/10.1021/acs.jced.2c00037
J. Chem. Eng. Data 2022, 67, 1365−1377

here. Conversely, the data of Shimoura et al. exhibit only negative deviations from the REFPROP EoS. The Δ_{AAD} values relative to the REFPROP EoS are 0.61% for this study and 0.43% for the study of Shimoura et al. However, Figure 6 shows that Shimoura's data exhibits a larger systematic deviation with temperature than the data of the present study. It is important to note that there is more than a 1% offset between the R-1234yf/134a speed of sound data reported in this study and the speed of sound data of Shimoura et al. where the data are reported at similar temperatures, pressures, and composition.

4. CONCLUSIONS

The liquid-phase speed of sound data are reported for binary mixtures of R-1234yf, R-134a, and R-1234ze(E) over the temperature range of 230−345 K to a maximum pressure of 51 MPa. For each binary mixture, data are reported for two nominal compositions of (0.33/0.67) and (0.67/0.33) mole fraction. The present study greatly expands the thermodynamic property database for the speed of sound of refrigerant blends. The data are compared to available Helmholtz-energy-explicit EoS mixture models without any adjustments. However, despite the lack of fine-tuning of the REFPROP models needed to provide accurate correlations for the present data, the Δ_{AAD} values are reasonable, ranging from 0.27 to 0.75%. Further adjustments to the available Helmholtz-energy-explicit EoS mixture models are needed to improve speed of sound calculations for the R-1234yf/134a, R-1234yf/1234ze(E), and R-134a/1234ze(E) mixtures. In future studies, the new speed of sound data along with bubble point and density data measured for the same mixtures by our group will be used to tune the current REFPROP mixture models. Of the available literature, the study of Shimoura et al. is the only study that reports speed of sound data that can be compared to the data reported in this study and only for a single mixture. The two data sources differ by more than 1%.

■ ASSOCIATED CONTENT

Supporting Information

The Supporting Information is available free of charge at https://pubs.acs.org/doi/10.1021/acs.jced.2c00037.

Raw unaveraged speed of sound data and fluid file file including the unpublished EoS of Lemmon and Akasaka (ZIP)

Short description of ZIP folder contents (PDF)

■ AUTHOR INFORMATION

Corresponding Author

Aaron J. Rowane − *Applied Chemicals and Materials Division, National Institute of Standards and Technology, Boulder, Colorado 80305, United States*; orcid.org/0000-0001-7605-0774; Email: Aaron.Rowane@nist.gov

Author

Richard A. Perkins − *Applied Chemicals and Materials Division, National Institute of Standards and Technology, Boulder, Colorado 80305, United States*; orcid.org/0000-0002-8526-6742

Complete contact information is available at: https://pubs.acs.org/10.1021/acs.jced.2c00037

Notes

The authors declare no competing financial interest.
Commercial equipment, instruments, or materials are identified only to adequately specify certain procedures. Such identification does not imply recommendation or endorsement by the National Institute of Standards and Technology, nor does it imply that the identified products are necessarily the best available for the purpose.

■ ACKNOWLEDGMENTS

We thank Megan Harries and Jason Widegren for providing analysis of the pure fluids used to prepare the binary mixtures studied in this work, Mark McLinden for his guidance in preparing the gas mixtures for the speed of sound measurements and technical discussions pertinent to this work, Ian Bell for his helpful technical discussions pertaining to the Helmholtz-energy-explicit EoS, and Eric Lemmon and Ryo Akasaka for providing the fluid file for the R-1234yf EoS. This work was supported by the Strategic Environmental Research and Development Program; Project WP19-1385: WP-2740 Follow-On: Low-GWP Alternative Refrigerant Blends for HFC-134a.

■ REFERENCES

(1) Calm, J. M. The next generation of refrigerants - Historical review, considerations, and outlook. *Int. J. Refrig.* **2008**, *31*, 1123−1133.

(2) McLinden, M. O.; Huber, M. L. (R)Evolution of refrigerants. *J. Chem. Eng. Data* **2020**, *65*, 4176−4193.

(3) Myhre, G.; Shindell, D. *Climate Change 2013 The Physical Science Basis: Chapter 8 Anthropogenic and Natural Radiative Forcing*; Cambridge University Press, 2014.

(4) McLinden, M. O.; Kazakov, A. F.; Brown, J. S.; Domanski, P. A. A thermodynamic analysis of refrigerants: Possibilities and tradeoffs for Low-GWP refrigerants. *Int. J. Refrig.* **2014**, *38*, 80−92.

(5) Domanski, P. A.; Brignoli, R.; Brown, J. S.; Kazakov, A. F.; McLinden, M. O. Low-GWP refrigerants for medium and high-pressure applications. *Int. J. Refrig.* **2017**, *84*, 198−209.

(6) Bell, I. H.; Domanski, P. A.; McLinden, M. O.; Linteris, G. T. The hunt for nonflamable refrigerant blends to replace R-134a. *Int. J. Refrig.* **2019**, *104*, 484−495.

(7) Bobbo, S.; Di Nicola, G.; Zilio, C.; Brown, J. S.; Fedele, F. Low GWP halocarbon refrigerants: A review of thermophysical properties. *Int. J. Refrig.* **2018**, *90*, 181−201.

(8) Bell, I. H.; Riccardi, D.; Bazyleva, A.; McLinden, M. O. Survey of data and models for refrigerant mixtures containing halogenated olefins. *J. Chem. Eng. Data* **2021**, *66*, 2335−2354.

(9) Al Ghafri, S. Z.; Rowland, D.; Arami-Niya, A.; Khamphasith, M.; Xiao, X.; Tsuji, T.; Tanaka, Y.; Seiki, Y.; May, E. F.; Hughes, T. J. Thermodynamic properties of hydrofluoroolefin (R1234yf and R1234ze(E)) refrigerant mixtures: Density vapour-liquid equilibrium, and heat capacity data and modelling. *Int. J. Refrig.* **2019**, *98*, 249−260.

(10) Higashi, Y. Measurements of thermodynamic properties for the 50 mass% R1234yf + 50 mass% R1234ze(E) blend. *Sci. Technol. Built. Environ.* **2016**, *22*, 1185−1190.

(11) Yotsumoto, Y.; Sugitani, R.; Matsuo, S.; Sotani, T. Density measurements of binary mixtures for (HFO-1234yf + HFC-134a) system. In *The 31st Japan Symposium on Thermophysical Properties*; Fukuoka, Japan, 2010.

(12) Chen, Q.; Qi, H.; Zhang, S.; Hong, R.; Chen, G. An experimental study of *PVTx* properties in the gas phase for binary mixtures of HFO-1234yf and HFC-134a. *Fluid Phase Equilib.* **2015**, *385*, 25−28.

https://doi.org/10.1021/acs.jced.2c00037
J. Chem. Eng. Data 2022, 67, 1365−1377

(13) Zhang, H.; Dong, X.; Zhong, Q.; Li, H.; Gong, M.; Shen, J.; Wu, J. Investigation of *pρTx* properties for R1234ze(E) + R134a mixtures in the gas phase. *Int. J. Refrig.* **2017**, *73*, 144−153.

(14) Kou, L.; Yang, Z.; Tang, Z.; Zhang, W.; Lu, J. Experimental measurements and correlation of isothermal vapor-liquid equilibria for HFC-32 + HFO-1234ze(E) and HFC-134a + HFO-1234ze(E) binary systems. *J. Chem. Thermodyn.* **2019**, *139*, 105798.

(15) Kamiaka, T.; Dang, C.; Hihara, E. Vapor-liquid equilibrium measurements for binary mixtures of R1234yf with R32, R125, and R134a. *Int. J. Refrig.* **2013**, *36*, 965−971.

(16) Akasaka, R.; Higashi, Y.; Yamada, Y. Thermodynamic properties of 1,1,1,2-tetrafluoroethane (R134a) + 2,3,3,3-tetrafluoropropene (R-1234yf) mixtures: Measurements of the critical parameters and a mixture model based on the multi-fluid approximation. *Int. J. Refrig.* **2015**, *58*, 146−153.

(17) Shimoura, H.; Matsuo, S.; Sotani, T. Speed of sound measurements in dense liquid of low GWP refrigerant mixture including HFO-1234yf. In *The 32nd Japan Symposium on Thermophysical Properties*; Yokohama, Japan, 2011.

(18) Richter, M.; McLinden, M. O.; Lemmon, E. W. Thermodynamic Properties of 2,3,3,3-Tetrafluoroprop-1-ene (R1234yf): Vapor Pressure and *p-ρ-T* Measurements and an Equation of State. *J. Chem. Eng. Data* **2011**, *56*, 3254−3264.

(19) Lin, C.-W.; Trusler, J. P. M. The speed of sound and derived thermodynamic properties of pure water at temperatures between (253 and 473) K and at pressures up to 400 MPa. *J. Chem. Phys.* **2012**, *136*, No. 094511.

(20) Lemmon, E. W.; Bell, I. H.; Huber, M. L.; McLinden, M. O. *NIST Standard Reference Database 23: Reference Fluid Thermodynamic and Transport Properties-REFPROP, Version 10.0*; National Institute of Standards and Technology: Gaithersburg, 2018.

(21) Tillner-Roth, R.; Baehr, H. D. An international standard formulation for the thermodynamic properties of 1,1,1,2-tetrafluoroethane (HFC-134a) for temperatures from 170 K to 455 K and pressures up to 70 MPa. *J. Phys. Chem. Ref. Data* **1994**, *23*, 657−729.

(22) Lemmon, E. W.; Akasaka, R. Unpublished equation of state, to be submitted to. J. Phys. Chem. Ref. Data, 2022.

(23) Thol, M.; Lemmon, E. W. Equation of state for thermodynamic properties of *trans*-1,3,3,3-tetrafluoropropene [R-1234ze(E)]. *Int. J. Thermophys.* **2016**, *37*, 28.

(24) Bell, I. H.; Lemmon, E. W. Automatic fitting of binary interaction parameters for multi-fluid helmholtz-energy-explicit mixture models. *J. Chem. Eng. Data* **2016**, *61*, 3752−3760.

(25) Outcalt, S. L.; Rowane, A. J. Bubble point measurements of mixtures of HFO and HFC refrigerants. *J. Chem. Eng. Data* **2021**, 4670.

(26) Harris, G. L., *Selected Laboratory ad Measurement Practices and Procedures to Support Basic Mass Calibrations*. NISTIR 6969; National Institute of Standards and Technology, 2003.

(27) McLinden, M. O.; Richter, M. Application of a two-sinker densimeter for phase-equilibrium measurements: A new technique for the detection of dew points and measurements on the (methane + propane) system. *J. Chem. Thermodyn.* **2016**, *99*, 105−115.

(28) Bruno, T. J.; Fortin, T. J.; Huber, M. L.; Laesecke, A.; Lemmon, E. W.; Mansfield, E.; McLinden, M. O.; Outcalt, S. L.; Perkins, R. A.; Urness, K. N.; Widegren, J. A. *Thermophysical Properties of Polyol Ester Lubricants*; NISTIR, 2019; Vol. *8263*, pp. 36−46.

(29) McLinden, M. O.; Perkins, R. A. A dual-path pulse echo instrument for speed of sound of liquids and dense gases and measurements on *p*-xylene and four halogenated-olefin refrigerants [R1234yf, R1234ze(E), R1233zd(E), and R1336mzz(Z)]. Manuscript in preparation, to be submitted to. *J. Chem. Thermodyn.* 2021.

(30) Ball, S. J.; Trusler, J. P. M. Speed of sound of *n*-hexane and *n*-hexadecane at temperatures between 298 and 373 K and pressures up to 100 MPa. *Int. J. Thermophys.* **2001**, *22*, 427−443.

(31) Meier, K.; Kabelac, S. Speed of sound instrument for fluids with pressures up to 100 MPa. *Rev. Sci. Instrum.* **2006**, *77*, 123903.

(32) Rowane, A. J. (2022) Speed of Sound Measurements of Binary Mixtures of 1,1,1,2-Tetrafluoroethane (R-134a), 2,3,3,3-Tetrafluoropropene (R-1234yf), and trans-1,3,3,3-Tetrafluoropropene (R-1234ze(E)) Refrigerants; National Institute of Standards and Technology, DOI: 10.18434/mds2-2555 (accessed 2022-05-03).